Negative Ion Chemistry of Ozone in the Gas Phase

Skip Williams,* Meghann F. Campos,† Anthony J. Midey,‡ Susan T. Arnold, Robert A. Morris, and Albert A. Viggiano

Air Force Research Laboratory, Space Vehicles Directorate, 29 Randolph Road, Hanscom AFB, Massachusetts 01731-3010

Received: July 30, 2001; In Final Form: October 1, 2001

A novel ozone source was developed to study the negative ion chemistry of ozone in the gas phase. Rate constants and product ion branching fractions are reported for 17 negative ion−molecule reactions involving ozone (O_3). This is the most comprehensive set of O_3 reactions with negative ions to date. The reactions proceed primarily through charge transfer and O atom transfer. The reaction rate constants for O^-, O_2^-, and OH^- are large and approximately equal to the thermal energy capture rate constant given by the Su-Chesnavich equation based on average dipole orientation theory. The negative ions NO_2^-, CO_4^-, SF_6^-, and PO_2^- are somewhat less reactive, reacting at approximately 20−50% of the thermal capture rate. The hydrofluorocarbon ions CF_3^- and $C_2F_5^-$ react at 80% of the thermal capture rate, and F^- is the major product ion formed. NO_3^-, CO_3^-, PO_3^-, CF_3O^-, F^-, Cl^-, and Br^- are found to be unreactive with rate constants $< 5 \times 10^{-12}$ cm^3 s^{-1}, which is the present detection limit of our apparatus using this ozone source. The I^- ion was observed to cluster with O_3 to form IO_3^- with a rate constant of approximately 1×10^{-11} cm^3 s^{-1}, which is a factor of 2 above our detection limit, and no other product channels were observed. All of the anions listed above showed no reactivity, $k < 5 \times 10^{-13}$ cm^3 s^{-1}, with O_2.

I. Introduction

Ionization in the wake flowfield behind bodies in hypersonic flight provides radar and optical characteristics that are usually determined by the chemistry occurring in the ionized wake region.[1] This region is a mixture of many different products, including polyatomic molecules, negative ions, and ablation products. Of these species, ozone (O_3) is of particular interest because it can attach electrons and is reactive with other negative ions. Negative ion−neutral reactions involving ozone are also important in atmospheric and plasma chemistry.[2−7] Despite the importance of ozone in these environments, a limited number of investigations of collisions of O_3 and negative ions have been performed, and the number of recent investigations is scarce. Various experimental techniques have been employed to study these reactions including flowing afterglow,[8−13] drift tube,[14] and ion beam methods.[15−18] However, the negative ion chemistry of ozone is not well resolved due to the scarcity of the data and discrepancies in reported rate constants and branching fractions.

To resolve some of these issues, a novel ozone source was developed to enable the facile study of the gas-phase negative ion chemistry of ozone. In this paper, rate constants and product ion branching fractions are reported for 17 negative ion−molecule reactions involving ozone. This is the most comprehensive set of O_3 reactions to date. The new measurements are discussed in the context of previous work where available.

II. Experimental Section

The measurements were made at 300 K using the selected-ion flow tube (SIFT) instrument at the Air Force Research Laboratory. This apparatus is described in detail elsewhere,[19,20] and the modifications required to perform experiments with ozone as a reactant gas are described here. The SIFT is shown schematically, with modifications, in Figure 1.

Ions are created in a remote, differentially pumped electron impact ion source that directs ions into a quadrupole mass filter where the ionic species of interest is mass selected. The mass-selected ions are injected via a Venturi-type inlet into a fast flow of helium carrier gas in a meter long stainless steel flow tube. Reactant gas is introduced into the flow tube through either of two stainless steel reactant gas inlets and allowed to react over a known distance at a known flow velocity. The SIFT operates at ca. 0.4 Torr helium buffer pressure, and the kinetics are observed over ca. 2 ms reaction time. A second quadrupole mass spectrometer resolves the reactant and the product ions, which are then detected by an electron multiplier. Extrapolations of product branching fractions to zero reactant flow yield the nascent branching fraction. The decay in the primary reactant ion signal as a function of increasing reactant gas flow rate yields the reaction rate constant. Concentrations are such that [buffer] ≫ [reactant neutral] ≫ [ions]. Under these conditions, pseudo-first-order kinetics apply, and the rate constant is given by

$$k = \frac{1}{[\mathrm{B}]\tau} \ln\left\{\frac{[\mathrm{A_o}^{\pm}]}{[\mathrm{A}^{\pm}]}\right\} \qquad (1)$$

where k is the rate constant, τ is the reaction time, [B] is reactant neutral concentration, $[\mathrm{A_o}^{\pm}]$ and $[\mathrm{A}^{\pm}]$ are the primary ion concentrations in the absence and presence of reactant neutral. The reaction time, τ, is the reaction distance divided by the buffer velocity multiplied by a correction factor determined from previous time-of-flight measurements that accounts for the fact that both the ion velocity and ion concentration are at a

* Corresponding author.
† Air Force Research Laboratory Space Scholars Program.
‡ Under contract to Visidyne Inc., Burlington, MA, 01803.

10.1021/jp012929r CCC: $22.00
Published on Web 01/17/2002

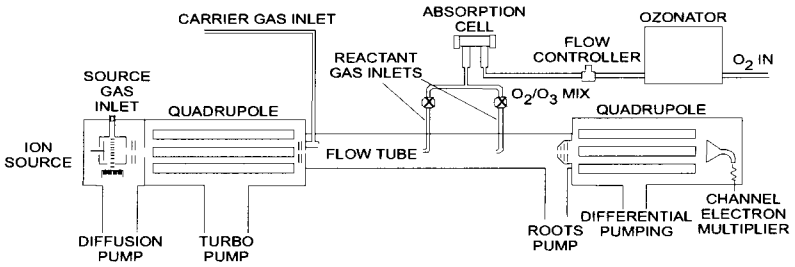

Figure 1. Overview of the selected ion flow tube (SIFT) with ozonator and absorption cell.

maximum along the axis of the flow tube. A typical value for the correction factor is 1.6. The buffer velocity is obtained from the mass flow rate of the buffer, the flow tube cross section, temperature, and pressure in the normal manner.[21] The absolute uncertainties of the rate constants are 25% and relative uncertainties are 15%.

An Orec O3V-0 ozonator was interfaced to the SIFT apparatus to produce the ozone reactant gas used in this experiment. A commercial supply of O_2 (Airco, 99.999%) was used to manufacture the ozone. The O_3 was produced at a pressure of 3−4 psig and using 0.9 A discharge current. The resulting reactant gas is approximately 5% O_3 in O_2, which is the same as that reported previously by Fahey et al.[11] The fraction of O_3 was relatively independent of the reactant gas flow rate over a 100 SCCM flow range. The presence of O_2 does not affect the measurements, because O_2 is unreactive with the negative ions studied here including product ions. Flow contamination was less than 0.5%, typically from nitrogen and carbon dioxide trace gases in the ozonator and the tubing. Contamination was minimized by flushing the lines and the ozonator regularly to prevent buildup of contaminants such as NO_2, NO_3, and CO_2. All fittings and valves used in the O_3 delivery system are stainless steel.

A flow controller regulates the reactant flow into a 10.2 cm long, 1.3 cm diameter Pyrex absorption cell fitted with quartz windows. The absorption cell is connected to the flow tube stainless steel reactant inlets by approximately 40 cm of 0.25 in. o.d. Teflon tubing. Varying the length of the Teflon tubing from 40 to 300 cm produced no difference (<5%) in the results, suggesting that no significant O_3 decomposition occurs in the tubing. The absolute concentration of O_3 is measured by optical absorption at 248 and 254 nm using a Perkin-Elmer Lambda 10 UV/vis spectrometer. The concentration of the ozone in the flow tube was found using

$$[O_3] = \left(\frac{2.303A}{\sigma_\lambda l}\right)\left(\frac{P_{FT}}{P_{AC}}\right)\left(\frac{F_{AC}}{F_{FT}}\right) \qquad (2)$$

where A is the log absorbance (base 10) output from the spectrometer, σ_λ is the absorption cross section for O_3 at wavelength λ (cm^2 $molecule^{-1}$), l is the length of the absorption cell in cm, P_{FT} is the flow tube pressure, P_{AC} is the absorption cell pressure, F_{AC} is the total flow through the absorption cell, and F_{FT} is the total flow through the flow tube. The 248 and 254 nm cross sections used were 1.08×10^{-17} and 1.137×10^{-17} cm^2 $molecule^{-1}$, respectively.[22,23]

III. Results

Reaction rate constants and product branching fractions for numerous negative ions reacting with O_3 measured at 300 K with the SIFT are shown in Table 1. Listed in Table 1 is the reaction of $C_2F_5^-$ with O_3, which proceeds at approximately 80% of the thermal capture rate and produces a large number of reaction product ions, some of which undergo secondary reactions with O_3. Because this reaction is relatively more complex than the others listed in Table 1, it is used as an example to illustrate the data acquisition and analysis procedures.

Figure 2 shows a sample primary ion decay plot for the reaction of $C_2F_5^-$ with both O_2 and O_3. The solid lines are nonlinear least-squares fits to the data performed to determine the rate constants according to eq 1. The $C_2F_5^-$ ion, like the other anions studied, does not exhibit any significant reactivity with O_2. The data plotted in Figure 2 show that the reaction rate constant for $C_2F_5^- + O_2$ is over 3 orders of magnitude smaller than that for $C_2F_5^- + O_3$. This reaction rate difference is more than enough to compensate for the fact that O_2 is being delivered to the flow tube at a concentration approximately 20 times greater than that of O_3. All of the ionic reactants listed in Table 1 showed a similar lack of reactivity, $k < 5 \times 10^{-13}$ cm^3 s^{-1}, with O_2. Therefore, the use of O_2 as the carrier gas to deliver O_3 to the flow tube does not interfere with the determination of rate constants and branching fractions. The use of O_2 as the carrier gas does greatly simplify the ozone generation and delivery requirements, ensuring fewer decomposition and contamination problems.

The normalized $C_2F_5^-$ counts as a function of O_3 concentration are replotted in Figure 3 along with the counts for the three major product channels of the $C_2F_5^- + O_3$ reaction. In Figure 3, the $C_2F_5^-$ reactant ion signal decreases by about a factor of 5 over the O_3 concentration range shown. Typical depletions of the reactant ion signal used in this study were in the factor of 4 to 20 range. The product count rates are summed and normalized to the total number of product counts to produce a branching fraction plot as a function of O_3 concentration as shown in Figure 4. In Figure 4, the F^- and O_3^- branching fractions increase with increasing O_3 concentration while the CF_3^- branching fraction decreases. This behavior is due to secondary reactions of the CF_3^- product ion with O_3. The CF_3^- ion reacts with O_3 to produce F^- (87%), O_3^- (12%), and a very minor amount of CF_3O^- (1%) as shown in Table 1. The small CF_3O^- and $C_2F_5O^-$ branching fractions are relatively independent of O_3 concentration, indicating that these ions are not significantly involved in any secondary chemical reactions. The solid lines shown in Figure 4 are linear least-squares fits performed to extrapolate to zero reactant flow to yield the nascent branching fractions that are reported in Table 1.

The reaction rate constants and product branching fractions of the negative ion reactions with O_3 listed in Table 1 represent an average of 3−10 independent data sets, such as that discussed above for $C_2F_5^- + O_3$. For all of the reactions studied, the neutral fragments generated are not measured, the most stable neutral products are assumed and recorded in Table 1. The standard heats of formation used in the calculations are from the NIST Chemistry WebBook.[24] In some cases, the count rates

TABLE 1: Reaction Rate Constants for Reactions of Ozone at 300 K Measured with the Selected Ion Flow Tube (SIFT)[a]

reaction	products	k;[k_c] (10^{-9} cm^3 s^{-1})	branching fractions	$-\Delta H$ kJ/mol
$O^- + O_3 \rightarrow$		*1.7*;[*1.5*]		
	$O_3^- + O$		0.81	63
	$O_2^- + O_2$		0.19	294
$O_2^- + O_3 \rightarrow$	$O_3^- + O_2$	*1.3*;[*1.2*]	1.00	160
$OH^- + O_3 \rightarrow$		*1.4*;[*1.4*]		
	$O_3^- + OH$		0.90	28
	$HO_2^- + O_2$		0.08	100
	$O_2^- + HO_2$		0.02	47
$NO_2^- + O_3 \rightarrow$		*0.18*;[*1.1*]		
	$NO_3^- + O_2$		0.99	264
	$O_3^- + NO_2$		0.01	−14
$NO_3^- + O_3 \rightarrow$	no reaction	<*0.005*;[*0.97*]		
	$NO_2^- + 2O_2$			21
$CO_3^- + O_3 \rightarrow$	no reaction	<*0.001*;[*0.98*]		
	$O_2^- + CO_2 + O_2$			98
$CO_4^- + O_3 \rightarrow$		*0.46*;[*0.93*]		
	$O_3^- + CO_2 + O_2$		0.93	81
	$CO_3^- + 2O_2$		0.07	108
$SF_6^- + O_3 \rightarrow$	$O_3^- + SF_6$	*0.22*;[*0.84*]	1.00	104
$PO_2^- + O_3 \rightarrow$	$PO_3^- + O_2$	*0.40*;[*0.97*]	1.00	326
$PO_3^- + O_3 \rightarrow$	no reaction	<*0.005*;[*0.92*]		
$CF_3^- + O_3 \rightarrow$		*0.76*;[*0.95*]		
	$F^- + CF_2O + O_2$		0.87	384
	$O_3^- + CF_3$		0.12	28
	$CF_3O^- + O_2$		0.01	556
$CF_3O^- + O_3 \rightarrow$	no reaction	<*0.004*;[*0.91*]		
$C_2F_5^- + O_3 \rightarrow$		*0.70*;[*0.86*]		
	$F^- + CF_2 + CF_2O + O_2$		0.56	144
	$CF_3^- + CF_2O + O_2$		0.37	360
	$O_3^- + C_2F_5$		0.04	29
	$CF_3O^- + O_2 + CF_2$		{0.03 for $CF_3O^- + C_2F_5O^-$}	316
	$C_2F_5O^- + O_2$			556
$F^- + O_3 \rightarrow$	No Reaction	<*0.002*;[*1.4*]		
	$FO^- + O_2$			4
$Cl^- + O_3 \rightarrow$	no reaction	<*0.002*;[*1.2*]		
	$ClO^- + O_2$			34
$Br^- + O_3 \rightarrow$	no reaction	<*0.005*;[*0.97*]		
	$BrO^- + O_2$			37
$I^- + O_3 \rightarrow$	IO_3^-	*0.01*;[*0.91*]	1.00	∼0
	$IO^- + O_2$			46

[a] The calculated collision rate constant, k_c, and the measured rate constant, k, are listed in italics. Energetics are taken from the NIST Chemistry WebBook.[24] Brackets indicte a product is too small to measure independently. All of the anions listed showed no reactivity, $k < 5 \times 10^{-13}$ cm^3 s^{-1}, with O_2.

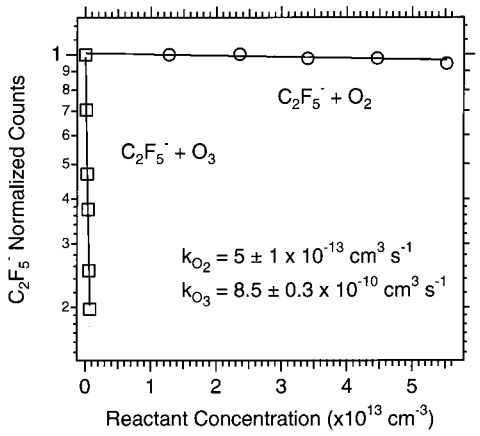

Figure 2. Normalized $C_2F_5^-$ counts plotted vs O_2 concentration (open circles) and O_3 concentration (open squares). The solid lines are nonlinear least-squares fits to the data performed to determine the rate constants according to eq 1. Experiments are performed with a reactant gas composition of 5% O_3 in O_2, which is possible since O_2 is unreactive.

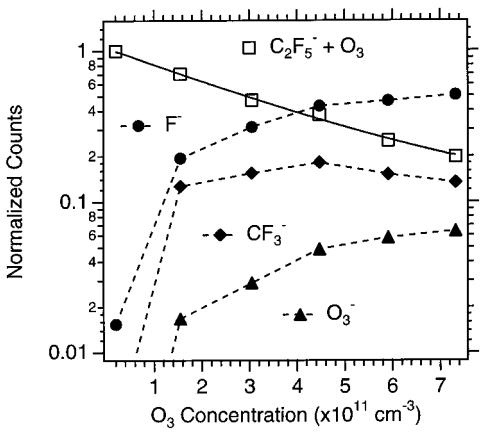

Figure 3. Normalized $C_2F_5^-$ (open squares), F^- (circles), CF_3^- (diamonds), and O_3^- (triangles) counts plotted vs O_3 concentration. The solid line is a nonlinear least-squares fit performed to determine the rate constants according to eq 1. The dashed lines are meant to guide the eye.

are too small to accurately determine the product branching fractions. For these reactions, the ionic products observed are listed in brackets to reflect this uncertainty.

IV. Discussion

SF_6^- Reaction. The reaction of SF_6^- with O_3 produces the charge-transfer product O_3^- exclusively. The measured charge-transfer rate constant is a factor of 7 larger than that measured

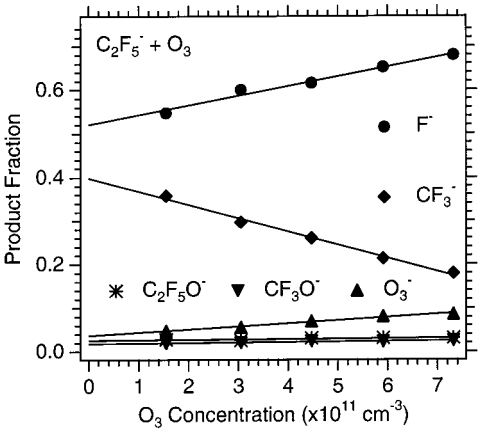

Figure 4. Product branching fractions for F^- (circles), CF_3^- (diamonds), O_3^- (triangles), CF_3O^- (inverted triangles), and $C_2F_5O^-$ (asterisks) plotted vs O_3 concentration. The solid lines are linear least-squares fits performed to extrapolate to zero reactant flow yielding the nascent branching fraction.

by Fehsenfeld,[8] a factor of 5 smaller than that reported more recently by Huey et al.,[12] and in good agreement with the recent measurement of 1.7×10^{-10} cm^3 s^{-1} reported by Catoire et al.[13] Huey et al. noted that the O_3 concentration was not measured directly in Fehsenfeld's experiments, because the focus of that work was to bracket the electron affinity of SF_6. Furthermore, Huey has remeasured the rate constant for this reaction at our request and obtained a value of 1.7×10^{-10} cm^3 s^{-1}, which is in excellent agreement with our value and that of Catoire et al.[25] Therefore, the discrepancy between the previously published rate constants and that reported in this work appears to be resolved.

The value of 2.2×10^{-10} cm^3 s^{-1} for the charge-transfer rate constant is more consistent with expectations based on the values of other exothermic charge-transfer reactions involving SF_6^- that have been found to be slow.[8,26,27] In particular, this value is consistent with the reported rate constants for the charge-transfer reactions of SF_6^- with NO_2 and Cl_2, which have electron affinities slightly larger than that of O_3.[12] This indicates that the dynamics of the charge transfer are controlled by conversion of SF_6^- to SF_6, rather than from the reactant partner. SF_6 and SF_6^- are known to have distinctly different geometries,[12] and the slow rate may be attributed to a kinetic barrier and/or poor Franck−Condon factors due to a large geometry change between the anion and neutral forms of SF_6.

This relatively slow charge-transfer rate facilitates the use of SF_6^- as a reagent for the detection of atmospheric species by chemical ionization mass spectrometry (CIMS). Huey at al. had ruled out such a possibility in their previous publication[12] based on the large charge-transfer rate constant reported in that work. The smaller value of the rate constant has allowed SF_6^- to be used as a CIMS reagent in recent measurements of pernitric acid gases in the upper troposphere and polar boundary layer.[25]

O^-, O_2^-, and OH^- Reactions. These species react with O_3 at the thermal energy capture rate constant given by the Su-Chesnavich equation.[28,29] The major reaction channel observed for all of these reactant ions was charge transfer, with oxygen atom transfer being the next most important channel. The reactions of O^-, O_2^-, and OH^- with O_3 have been studied previously in flowing afterglow and ion beam apparatuses. Our results are in reasonable agreement with the flowing afterglow results of Dotan et al.[14,30,31] and Ferguson and co-workers.[2] Specifically, these authors report charge-transfer rate constants of 8×10^{-10} cm^3 s^{-1}, 6×10^{-10} cm^3 s^{-1}, and 9×10^{-10} cm^3 s^{-1} for reactions of O^-, O_2^-, and OH^- with O_3, respectively. Furthermore, the rate constant measured in this work for $O_2^- + O_3$ is in good agreement with the recent measurement of 6.3×10^{-10} cm^3 s^{-1} reported by Catoire et al.[13] and 7.8×10^{-10} cm^3 s^{-1} reported by Fahey et al.[11] However, all of the flowing afterglow values are about 1/2 to 2/3 of the present values. No obvious reasons are apparent for the discrepancies among the rate constants. However, the good agreement of our SF_6^- rate constant with two recent measurements of that reaction lend credibility to the present measurements. In addition, other reactive channels were observed in the present SIFT work for O^- and OH^- reactions that were not reported in the previous flowing afterglow work. In the flowing afterglow experiments only the charge transfer products were observed, but other minor product channels were probably missed due to the presence of more than one primary ion in those experiments.

Ion beam measurements made at elevated kinetic energy reported rate coefficients that are significantly lower than those reported here. Lifshitz and co-workers[16,17] report total rate constants at a laboratory collision energy of ca. 0.3 eV of 5.1×10^{-10} cm^3 s^{-1} and 5.4×10^{-10} cm^3 s^{-1} for the reactions of O^- and OH^- with O_3, respectively. These lower values may reflect an energy dependence in the rate constant. Alternatively, the collection of charge-transfer products in a beam-cell apparatus is difficult, and the discrepancy may be a result of this experimental condition. However, the branching fractions reported from the beam experiments for the $OH^- + O_3$ reaction, namely,

$$OH^- + O_3 \rightarrow O_3^- + OH \quad (0.92)$$

$$HO_2^- + O_2 \quad (0.06)$$

$$O_2^- + HO_2 \quad (0.02)$$

are in excellent agreement with the present results. For the reaction of O^- with O_3, however, Lifshitz and co-workers[16,17] report the following,

$$O^- + O_3 \rightarrow e^- + 2O_2 \quad (0.59)$$

$$O_3^- + O \quad (0.39)$$

$$O_2^- + O_2 \quad (0.02)$$

which is in poor agreement with the presently measured branching fractions, because no reactive detachment was observed for the reaction of O^- with O_3 in the SIFT. Electron detachment is straightforward to detect in the SIFT apparatus, because it is associated with a reduction in the nose cone current, which is continuously monitored.[32] Therefore, the disagreement with the beam experiments may indicate an energy dependence. The abundance of electron attachment at higher energies may be a result of a multistep process where O_2^- is formed with enough energy to lose an electron at 0.3 eV but not at room temperature. The predominance of the charge-transfer channel over the atom transfer channel in the beam experiments is in agreement with the present results.

NO_2^- and PO_2^- Reactions. The dominant reaction channel observed for NO_2^- and PO_2^- reacting with O_3 was oxygen atom transfer, i.e., oxidation of the reactant ion to anions with very high detachment energies. A minor amount, 1%, of the charge-transfer product was observed in the $NO_2^- + O_3$ reaction. The

measured rate constant for the reaction of PO_2^- with O_3 is approximately half the thermal capture rate constant despite the large exothermicity associated with that reaction. There are no other measurements available for comparison for the $PO_2^- + O_3$ reaction. The NO_2^- anion reacts slower at 1.8×10^{-10} cm^3 s^{-1} and is also associated with a large exothermicity. Dotan et al.[30,31] and Ferguson and co-workers[2] studied this reaction in a flowing afterglow apparatus and observed oxygen atom transfer as the major product channel with rate constants of 1.2×10^{-10} cm^3 s^{-1} and 0.9×10^{-10} cm^3 s^{-1}, respectively, which is in reasonable agreement with the present measurements. However, as with the reactions discussed above, the rate constants are about 1/2 to 2/3 of the present value, and the minor reaction channel was not reported.

Given the electron affinities of NO_2 and O_3 of 2.27 eV[33] and 2.10 eV,[33,34] respectively, the charge-transfer reaction channel is endothermic at thermal collision energies. This is supported by the fact that the charge-transfer rate constant reported here is only 1.8×10^{-12} cm^3 s^{-1}. The maximum value for the rate constant can be estimated as the collision rate times $e^{-\Delta H/RT}$ or 3×10^{-12} cm^3 s^{-1}. The good agreement between these two numbers suggests that the charge transfer is very efficient once enough energy is available.

The $NO_2^- + O_3$ reaction was also studied using ion beam methodology by Lifshitz and co-workers.[17] At 0.3 eV laboratory collision energy, these authors reported that charge transfer was the major reaction channel,

$$NO_2^- + O_3 \rightarrow NO_2 + O_3^-$$

in contrast to the oxygen atom transfer observed in the flow tube experiments. The rate constant reported by Lifshitz et al. was 9×10^{-11} cm^3 s^{-1}. At the collision energies studied by Lifshitz et al., the charge-transfer reaction is energetically feasible, which may explain the predominance of this channel under their conditions.

The reaction of O_3^- with NO_2 is known to produce NO_3^-, and charge transfer is possible in the ion−neutral collision complex since the reaction is only 16.4 kJ/mol (0.17 eV) endothermic. This fact, coupled with the observed efficiency of charge transfer when energetically feasible, may indicate that at least some of the reaction proceeds through a two-step mechanism, i.e., charge transfer followed by O transfer. Future drift tube experiments may provide the information necessary to resolve the mechanism of this reaction.

CO_4^- Reaction. The reaction of CO_4^- with O_3 proceeds at approximately half the thermal energy capture rate producing primarily the charge-transfer product, O_3^-, with a minor amount of CO_3^-. Fehsenfeld and Ferguson[2,9] studied this reaction in a flowing afterglow apparatus and obtained a rate constant for charge transfer of 1.3×10^{-10}cm^3 s^{-1}, which is about a factor of 3 lower than our value, and no CO_3^- products were observed. In the experiments performed by Fehsenfeld and Ferguson,[9] the relative reactivity between the CO_4^- and the known reactivity of O^-, O_2^-, and NO_2^- with O_3 at the time of their publication was used to determine the reported rate constant for CO_4^-. The absolute rate constant determined by these authors is limited by the accuracy of the earlier determinations of the reference reactions, which as noted above, are lower than those reported in the present work. Catoire et al. have directly measured this rate constant and obtained a value of 3.4×10^{-10} cm^3 s^{-1} and recalculated the value of Fehsenfeld and Ferguson[2,9] using the more recent flowing afterglow values for the $O_2^- + O_3$ reaction and obtained a value of 3.0×10^{-10} cm^3 s^{-1}.[13] Again, these values are approximately 2/3 of the present values obtained in the SIFT. Furthermore, Catoire et al. were unable to detect the presence of the CO_3^- product channel due to the high concentrations of CO_2 in the flow tube required to generate the CO_4^- reactant ion, which converted all of the O_3^- to CO_3^-.

CF_3^- and $C_2F_5^-$ Reactions. Both these ions react at approximately 80% of the thermal energy capture rate constant, and only a minor amount of charge transfer is observed. The charge-transfer reaction channel is only exothermic by 27−28 kJ/mol which may account for the fact that reactive channels dominate. The main product channel in both reactions involves the production of F^-. Small oxidation channels producing CF_3O^- and $C_2F_5O^-$ are also observed. Another major product channel is observed in the $C_2F_5^-$ reaction, namely, CF_3^-.

The following mechanism may account for the reactivity of CF_3^- and $C_2F_5^-$. First ozone attaches to CF_3^- or $C_2F_5^-$. This complex formation step is followed by rapid O_2 release, leaving CF_3O^- or $C_2F_5O^-$. However, the initial CF_3O^- or $C_2F_5O^-$ produced are internally excited and may be relaxed to the ground state or decompose. A C−F bond can rupture and the major F^- product is formed. If the C−C bond in $C_2F_5O^-$ breaks, $CF_3^- + CF_2O$ is formed. All these channels are highly exothermic. The sum of the CF_3^- and F^- channels is approximately equal to the F^- channel in the CF_3^- reaction, an indication of potentially similar mechanisms. To form CF_3O^- in the $C_2F_5^-$ reaction, an F^- may transfer from CF_3^- to CF_2O.

NO_3^-, CO_3^-, PO_3^-, CF_3O^-, F^-, Cl^-, Br^-, and I^- Reactions. All these anions with the exception of I^- are found to be unreactive with rate constants $< 5 \times 10^{-12}$ cm^3 s^{-1}, consistent with previous observations.[2,9,11,12,17] While charge transfer is endothermic for all these ions, most of the reactions do have exothermic channels involving O atom transfer that are not observed, most likely because they are spin forbidden. Lifshitz and co-workers studied[35] the translational energy dependence of the halogen anions F^-, Cl^-, Br^-, and I^- with O_3 up to 6 eV laboratory energy and observed charge transfer (O_3^- product) with thresholds in the 1.1 to 1.3 eV center of mass (CM) energy range. The O atom transfer channels were not observed in this energy regime, indicating that a singlet−triplet conical intersection is lacking or is associated with significant barriers preventing the production of FO^-, ClO^-, BrO^-, and IO^-. However, the I^- ion was observed to cluster with O_3 with a rate constant of approximately 1×10^{-11} cm^3 s^{-1}, which is only a factor of 2 above our detection limit, and no other product channels were observed. The possibility of IO^- production followed by O_2 clustering to produce IO_3^- is unlikely based on the observation of Lifshitz and co-workers[35] and due to the weak clustering of O_2 to negative ions.[36] The reactions of O_3 with NO_3^- and CO_3^- are associated with exothermic channels involving O atom transfer from the negative anion. These reaction channels are also spin forbidden and most likely involve multiple steps, and hence, are not observed within the detection limit of these experiments.

V. Summary

Numerous negative ions reacting with O_3 were studied at 300 K in a selected-ion flow tube coupled to a novel ozone source. The reactions proceed primarily through charge transfer and O atom transfer. However, some of the reactions, such as those involving CF_3^- and $C_2F_5^-$, exhibit a rich chemistry with at least several products being produced. The reaction rate constants for O^-, O_2^-, and OH^- are large and approximately equal to

TABLE 2: Comparison of the Previous Reaction Rate Constants Measurements to the Present Work for Reactions of Ozone at 300 K (see text for discussion)

reaction	products	k (10^{-9} cm^3 s^{-1}) present SIFT	k (10^{-9} cm^3 s^{-1}) previous flowing afterglow	k (10^{-9} cm^3 s^{-1}) previous ion beam
$SF_6^- + O_3 \rightarrow$	$O_3^- + SF_6$	0.22	0.17[d], 0.17[c], 1.2[b], 0.032[a]	
$O^- + O_3 \rightarrow$	$O_3^- + O$	1.4	0.8[f]	0.2[j]
	$O_2^- + O_2$	0.3		0.01[j]
	$e^- + 2O_2$	<0.005		0.3[j]
$O_2^- + O_3 \rightarrow$	$O_3^- + O_2$	1.3	0.63[d], 0.78[h], 0.6[f,g]	
$OH^- + O_3 \rightarrow$	$O_3^- + OH$	1.3	0.9[f]	0.5[j]
	$HO_2^- + O_2$	0.1		0.03[j]
	$O_2^- + HO_2$	0.03		0.01[j]
$NO_2^- + O_3 \rightarrow$	$NO_3^- + O_2$	0.18	0.12[f], 0.09[g]	Not Observed
	$O_3^- + NO_2$	0.002		0.09[k]
$CO_4^- + O_3 \rightarrow$	$O_3^- + CO_2 + O_2$	0.43	0.34[d], 0.13[g,i]	
	$CO_3^- + 2O_2$	0.03		

[a] Reference 8. [b] Reference 12. [c] Reference 25. [d] Reference 13. [f] References 14, 31, and 30. [g] Reference 2. [h] Reference 11. [i] Reference 9. [j] Reference 16. [k] Reference 17.

the thermal energy capture rate constant given by the Su-Chesnavich equation. The negative ions NO_2^-, CO_4^-, SF_6^-, and PO_2^- are somewhat less reactive, reacting at approximately 20−50% of the thermal capture rate. The hydrofluorocarbon ions CF_3^- and $C_2F_5^-$ react at 80% of the thermal capture rate, and F^- is the major product ion formed. The NO_3^-, CO_3^-, PO_3^-, CF_3O^-, F^-, Cl^-, and Br^- anions are found to be unreactive with rate constants $< 5 \times 10^{-12}$ cm^3 s^{-1}. The I^- ion was observed to cluster with O_3 with a rate constant of approximately 1×10^{-11} cm^3 s^{-1}, which is a factor of 2 above our detection limit using this ozone source, and no other product channels were observed. Furthermore, all of the anions examined are unreactive with O_2, i.e., no products observed, with rate constants $< 5 \times 10^{-13}$ cm^3 s^{-1} within the detection limits of our method.

The reaction rate data that has been reported by more than one source are summarized in Table 2. It is clear from the inspection of Table 2 that the literature values regarding the negative ion chemistry of ozone, prior to this study, lacked sufficient agreement for application to detailed physical models. For the reaction of SF_6^- with ozone, there is now good agreement between three recent measurements, indicating reliable delivery and knowledge of the O_3 concentrations in the present experiment. For other reactions, the present measurements are in reasonable agreement with previous flowing afterglow measurements, with the older measurements being typically 30−50% lower than the present results. The present experiments have cleaner source conditions and limited secondary chemistry and should be the more accurate of the data reported. There is poor agreement with rate data obtained using ion beam methods at elevated energies. This discrepancy is due, at least in part, to the different energy regime studied and to the collection efficiency considerations in the beam-cell experiments. The values reported in Table 1 represent the most self-consistent and complete set of reaction rate and branching fraction data reported to date and based on the above considerations are recommended for use in modeling applications requiring thermal rate data near 300 K.

Acknowledgment. We thank John Williamson and Paul Mundis for technical support. We thank L. Gregory Huey for the early communication of the revised $SF_6^- + O_3$ results. We thank Berk Knighton for helpful discussions. This work was supported by AFOSR under Tasks 2303EP4. A.J.M. was supported through Visidyne contract number F19628-99-C-0069.

References and Notes

(1) Sutton, E. A. *AIAA J.* **1968**, *6*, 1873.
(2) Ferguson, E. E. Ion−Molecule Reactions in the Atmosphere. In *Kinetics of Ion−Molecule Reactions*; Ausloos, P., Ed.; Plenum Publishing Corp.: New York, 1979; p 377.
(3) Ferguson, E. E. *Acc. Chem. Res.* **1970**, *3*, 402.
(4) Wong, A. Y.; Steinhauer, J.; Close, R.; Fukuchi, T.; Milikh, G. M. *Comments Plasma Phys. Controlled Fusion* **1989**, *12*, 223.
(5) Dalgarno, A.; Fox, J. Ion chemistry in atmospheric and astrophysical plasmas. In *Unimolecular and Bimolecular Ion−Molecule Reaction Dynamics*; Ng, C.-Y., Baer, T., Powis, I., Eds.; Wiley: New York, 1994; p 1.
(6) Richter, R.; Lindinger, W. "Ion−molecule reactions pertaining to etching plasmas"; Symposium on Atomic and Surface Physics, 1986, Obertraun, Austria.
(7) Smith, D.; Adams, N. G. *Pure Appl. Chem.* **1984**, *56*, 175.
(8) Fehsenfeld, F. C. *J. Chem. Phys.* **1971**, *54*, 438.
(9) Fehsenfeld, F. C.; Ferguson, E. E. *J. Chem. Phys.* **1974**, *61*, 3181.
(10) Fehsenfeld, F. C.; Crutzen, P. J.; Schmeltekopf, A. L.; Howard, C. J.; Albritton, D. L.; Ferguson, E. E.; Davidson, J. A.; Schiff, H. I. *J. Geophys. Res.* **1976**, *81*, 4454.
(11) Fahey, D. W.; Bohringer, H.; Fehsenfeld, F. C.; Ferguson, E. E. *J. Chem. Phys.* **1982**, *76*, 1799.
(12) Huey, L. G.; Hanson, D. R.; Howard, C. J. *J. Phys. Chem.* **1995**, *99*, 5001.
(13) Catoire, V.; Stepien, C.; Labonnette, D.; Rayez, J.-C.; Rayez, M.-T.; Poulet, G. *Phys. Chem. Chem. Phys.* **2001**, *3*, 193.
(14) Dotan, I.; Davidson, J. A.; Streit, G. E.; Albritton, D. L.; Fehsenfeld, F. C. *J. Chem. Phys.* **1977**, *67*, 2874.
(15) Rutherford, J. A.; Turner, B. R.; Vroom, D. A. *J. Chem. Phys.* **1973**, *58*, 5267.
(16) Lifshitz, C.; Wu, R. L. C.; Haartz, J. C.; Tiernan, T. O. *J. Chem. Phys.* **1977**, *67*, 2381.
(17) Lifshitz, C.; Wu, R. L. C.; Riernan, T. O.; Terwilliger, D. T. *J. Chem. Phys.* **1978**, *68*, 247.
(18) Fedchak, J. A.; Peko, B. L.; Champion, R. L. *J. Chem. Phys.* **1995**, *103*, 981.
(19) Viggiano, A. A.; Morris, R. A.; Dale, F.; Paulson, J. F.; Giles, K.; Smith, D.; Su, T. *J. Chem. Phys.* **1990**, *93*, 1149.
(20) Viggiano, A. A.; Morris, R. A. *J. Phys. Chem.* **1996**, *100*, 19227.
(21) Ferguson, E. E.; Fehsenfeld, F. C.; Schmeltekopf, A. L. Flowing afterglow measurements of ion−neutral reactions. In *Advanced Atomic Molecular Physics*; Bates, D. R., Ed.; Academic: New York, 1969; Vol. 5, p 1.
(22) Mauersberger, K.; Barnes, J.; Hanson, D.; Morton, J. *J. Geophys. Res. Lett.* **1986**, *13*, 671.
(23) DeMore, W. B.; Sander, S. P.; Golden, D. M.; Molina, M. J.; Hampson, R. F.; Kurylo, M. J.; Howard, C. J.; Ravishankara, A. R. *Chemical Kinetics and Photochemical Data for Use in Stratospheric Modeling*, JPL Publication 90-1, Jet Propulsion Laboratory, 1990.
(24) *NIST Chemistry WebBook, NIST Standard Reference Database No. 69*; Mallard, W. G.; Linstrom, P. J., Eds.; National Instututes of Standards and Technology: Gaithersburg, MD, 2001; Vol. (http://webbook.nist.gov/chemistry).
(25) Huey, L. G., private communication, 2001.
(26) Streit, G. E. *J. Chem. Phys.* **1982**, *77*, 826.
(27) Grimsrud, E. P.; Chowdhury, S.; Kebarle, P. *J. Chem. Phys.* **1985**, *83*, 1059.
(28) Su, T.; Chesnavich, W. J. *J. Chem. Phys.* **1982**, *76*, 5183.
(29) Su, T. *J. Chem. Phys.* **1988**, *89*, 5355.

(30) Dotan, I.; Albritton, D. L.; Fehsenfeld, F. C., unpublished results.

(31) Ikezoe, Y.; Matsuoka, S.; Takebe, M.; Viggiano, A. A. *Gas Phase Ion−Molecule Reaction Rate Constants Through 1986*; Maruzen Company, Ltd.: Tokyo, 1987.

(32) Van Doren, J. M.; Viggiano, A. A.; Morris, R. A.; Miller, A. E. S.; Miller, T. M.; Paulson, J. F.; Deakyne, C. A.; Michels, H. H.; Montgomery, J. A., Jr. *J. Chem. Phys.* **1993**, *98*, 7940.

(33) Lias, S. G.; Bartmess, J. E.; Liebman, J. F.; Holmes, J. L.; Levin, R. D.; Mallard, W. G. Ion Energetics Data. In *NIST Chemistry WebBook, NIST Standard Reference Database Number 69*; Mallard, W. G., Linstrom, P. J., Eds.; NIST: Gaithersburg, 1998; (http://webbook.nist.gov).

(34) Arnold, D. W.; Xu, C. S.; Kim, E. H.; Neumark, D. M. *J. Chem. Phys.* **1994**, *101*, 912.

(35) Lifshitz, C.; Wu, R. L. C.; Tiernan, T. O.; Terwilliger, D. T. *J. Chem. Phys.* **1978**, *68*, 247.

(36) Keesee, R. G.; Castleman, A. W., Jr. *J. Phys. Chem. Ref. Data* **1986**, *15*, 1011.